

Four-terminal Josephson junctions: diode effects, anomalous currents and transverse currents

Bijay Kumar Sahoo¹ and Abhiram Soori^{1,*}

¹*School of Physics, University of Hyderabad, Prof. C. R. Rao Road, Gachibowli, Hyderabad-500046, India*

We study a multi-terminal Josephson junction consisting of a central spin-orbit-coupled region with an in-plane Zeeman field connected to four superconducting terminals. This setup allows for the simultaneous measurement of both longitudinal and transverse Josephson currents in response to a phase bias and provides a platform to probe the planar Hall effect in superconducting transport. We find that the system exhibits the anomalous Josephson effect (AJE) and the Josephson diode effect (JDE) when the symmetry between opposite momentum modes is broken. Specifically, breaking the symmetry between k_x and $-k_x$ results in JDE and AJE in the longitudinal Josephson current, while breaking the symmetry between k_y and $-k_y$ leads to a finite transverse Josephson current that also exhibits JDE and AJE. Furthermore, for specific parameter choices, the current-phase relation in the transverse direction supports unidirectional transport, highlighting its potential for superconducting circuit applications. Our setup offers a new route to engineering nonreciprocal superconducting transport.

Introduction .- A nonsuperconducting material sandwiched between two superconductors (SCs) can carry an equilibrium current when a phase difference exists between the superconductors. This phenomenon, known as the Josephson effect [1], arises due to bound states within the superconducting gap that transport current under a phase bias [2]. The dependence of this current on the phase difference defines the current-phase relation (CPR), with its extrema termed critical currents. If a Josephson junction breaks both time-reversal (TR) and inversion (I) symmetries, the critical currents become asymmetric, leading to the Josephson diode effect (JDE). This effect has recently attracted significant theoretical and experimental interest [3–13]. In systems with spin-orbit coupling (SOC) and a Zeeman field, both I and TR symmetries are broken, leading to magnetochiral anisotropy, where left- and right-moving electrons acquire unequal velocities. This anisotropy has been linked to JDE observed in spin-orbit-coupled systems [4, 5].

On the other hand, in planar Hall effect (PHE), a transverse voltage emerges in response to a longitudinal current in a two-dimensional electron gas with strong SOC and an in-plane magnetic field [14–18]. Unlike the conventional Hall effect, which originates from the Lorentz force, PHE results from the interplay of the Zeeman field and SOC [19, 20].

While Josephson junctions with spin-orbit-coupled materials under a Zeeman field have been extensively studied [9, 21, 22], the possibility of transverse currents in such setups remains largely unexplored. However, transverse current has been theoretically shown to exist in normal metal-superconductor junctions with interfacial SOC [23] and in Josephson junctions on topological insulator surface states under an in-plane Zeeman field [24]. However, it is not clear how these transverse currents can be measured. Furthermore, multi-terminal Joseph-

son junctions have been experimentally realized [25].

Motivated by these developments, we propose a Josephson junction setup involving a spin-orbit-coupled two-dimensional electron gas, where transverse currents can be measured in a multi-terminal configuration. In our design, two superconductors are connected longitudinally at opposite ends of the system, while two additional superconductors are attached in the transverse direction, as shown in Fig. 1. While the current in the transverse terminals serves as a direct probe of transverse Josephson currents, the currents in the terminals in the longitudinal direction serve to probe the usual CPR and associated anomalous Josephson effect (AJE) and JDE. While superconducting phases on the left and the right terminals are $\phi_s/2$ and $-\phi_s/2$, the transverse terminals are maintained at zero superconducting phase.

System .- The system under study consists of a central spin-orbit-coupled (SOC) region connected to four superconducting blocks, as shown in Fig. 1. We model the system using a tight-binding approach on a square lattice. The total Hamiltonian of the system is given by

$$H = H_L + H_{LS} + H_{SOC} + H_{SR} + H_R + H_B + H_{BS} + H_{ST} + H_T, \quad (1)$$

where H_L , H_R , H_T , and H_B represent the Hamiltonians of the left (L), right (R), top (T), and bottom (B) superconducting blocks, respectively. The term H_{SOC} describes the Hamiltonian of the central SOC region. An in-plane Zeeman field is applied to the SOC region. The coupling between each superconducting block and the SOC region is represented by H_{pS} , where $p = L, R, T, B$. The block L (R) is maintained at phase $\phi_s/2$ ($-\phi_s/2$) and the blocks T, B are maintained at phase 0. The exact form of these Hamiltonians is detailed in Appendix A.

The Josephson currents J_p (for $p = L, R, T, B$) at the junctions between the central SOC region and the superconducting blocks are computed as described in Appendix B. The system is designed in such a way that

* abhirams@uohyd.ac.in

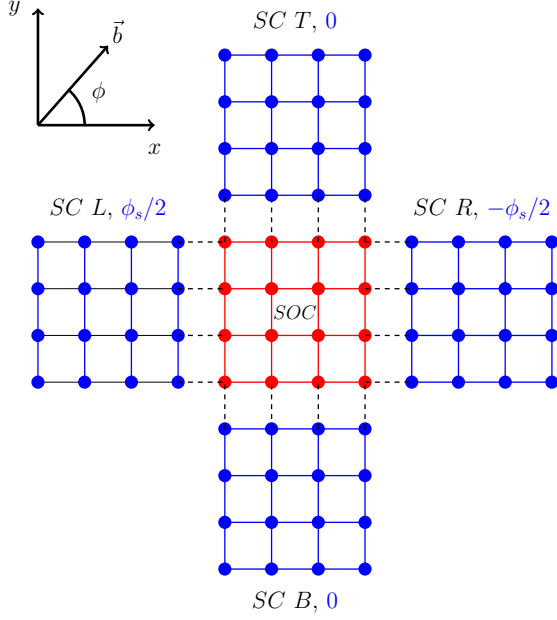


FIG. 1. Schematic diagram of the proposed setup. SC on the left (right) is maintained at a phase $\phi_s/2$ ($-\phi_s/2$). SCs on top and bottom are maintained at phase 0. An in-plane Zeeman field is applied to the central SOC region.

when either the SOC or the Zeeman field is switched off, there is no net current that flows into the terminals- T and B .

Results.- Using experimentally relevant parameters [9], we perform numerical calculations. The hopping amplitude is set to $t = 3.8$ meV, with chemical potentials in the SC and spin-orbit-coupled (SOC) regions given by $\mu_s = \mu_c = -3.6t$. The SOC strength is $\alpha = 0.5t$, the superconducting pairing potential is $\Delta = 0.06t$, and the Zeeman energy is $b = 0.1t$. The system consists of a central SOC region and four SC blocks, each modeled as a 6×6 square lattice. The currents flowing into (out of) the top/right (J_T, J_R) and bottom/left (J_B, J_L) superconductors satisfy Kirchhoff's current law. Additionally, the relations $J_L = J_R$ ($= J_x$) and $J_T = J_B$ ($= J_y$) hold due to the symmetry of the setup and the chosen SC phase configuration.

In Fig. 2, the CPRs for longitudinal and transverse currents (J_x and J_y) are plotted for a Zeeman field of strength $b = 0.1t$ oriented at an angle $\phi = \pi/3$ with respect to the x -axis. Due to the involvement of three SC phases ($\phi_s, 0, -\phi_s$), the CPRs exhibit a 4π -periodicity. Both the longitudinal and the transverse currents display AJE and JDE. The Hamiltonian for the central SOC region in momentum space is given by

$$H(\mathbf{k}) = \epsilon_k \sigma_0 + \alpha(\sin k_x \sigma_y - \sin k_y \sigma_x) + b(\cos \phi \sigma_x + \sin \phi \sigma_y), \quad (2)$$

where $\epsilon_k = -2t(\cos k_x + \cos k_y) - \mu_c$. For $\phi \neq \pi/2, 3\pi/2$, the asymmetry between k_y and $-k_y$ leads to a finite

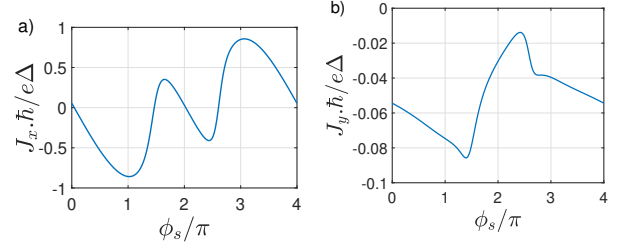


FIG. 2. CPR: (a) longitudinal Josephson current (b) transverse Josephson current. Parameters: $\alpha = 0.5t$, $b = 0.1t$, $\Delta = 0.06t$, $\phi = \pi/3$, $\mu_c = \mu_s = -3.6t$. The number of sites in x and y -directions for SC (L_s^x, L_s^y) and SOC (L_c^x, L_c^y) regions are $L_s^x = L_s^y = L_c^x = L_c^y = 6$.

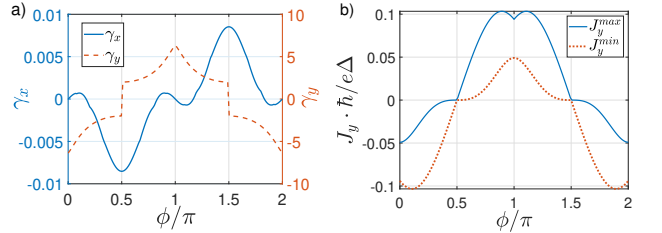


FIG. 3. a) Diode effects coefficient for longitudinal (transverse) CPR γ_l (γ_t) versus ϕ -the angle made by the in-plane Zeeman field with x -direction. b) Transverse critical currents versus magnetization angle ϕ . Other parameters are the same as in Fig. 2.

transverse current. Similarly, for $\phi \neq 0, \pi$, the asymmetry between k_x and $-k_x$ results in JDE and AJE [26, 27]. Notably, Fig. 2 reveals that the transverse Josephson current is unidirectional for this parameter set.

To quantify the diode effect, we define the longitudinal and transverse diode coefficients as

$$\gamma_d = \frac{2(J_d^{\max} + J_d^{\min})}{J_d^{\max} - J_d^{\min}}, \quad d = x, y. \quad (3)$$

Figure 3 plots γ_x and γ_y as functions of ϕ , the angle of the in-plane Zeeman field. As expected, the longitudinal diode effect vanishes at $\phi = 0, \pi$, while the transverse diode effect disappears at $\phi = \pi/2, 3\pi/2$. Additionally, Fig. 3(b) shows the variation of transverse critical currents with ϕ , demonstrating that the transverse current remains unidirectional and vanishes at $\phi = \pi/2, 3\pi/2$. In the range $\phi \in [\pi/2, \pi]$, the increasing asymmetry between k_y and $-k_y$ leads to a monotonic dependence of the transverse diode coefficient on ϕ . A similar argument explains the overall behaviour of the transverse diode effect coefficient across the entire range of ϕ .

We plot the longitudinal anomalous Josephson current (J_x^A) and transverse anomalous Josephson current (J_y^A) versus magnetization angle ϕ in Fig. 4 for the same set of parameters as in Fig. 3. Here, we can see that J_x^A and J_y^A vary sinusoidally versus the magnetization angle ϕ , which is a direct consequence of the combination of SOC and the Zeeman field. And J_x^A is zero for $\phi = 0, \pi$, because at

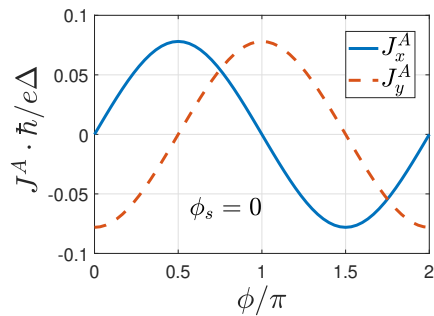


FIG. 4. Longitudinal and Transverse anomalous Josephson current versus magnetization angle ϕ . Other parameters are the same as in Fig. 2.

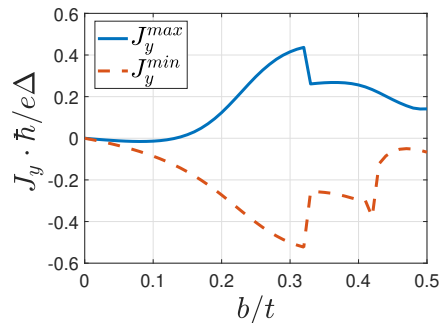


FIG. 5. Transverse critical Josephson currents J_y^{max} and J_y^{min} versus the Zeeman energy b for $\phi = \pi/4$. Other parameters are the same as in Fig. 2.

these values of ϕ , the y -component of the Zeeman field is zero and hence the symmetry between k_x and $-k_x$ modes is not broken. Similarly, the transverse current is zero for $\phi = \pi/2, 3\pi/2$ as the x component of the Zeeman field is zero at these values of ϕ and the symmetry between k_y and $-k_y$ is not broken. Notably, if the curve for J_x^A is shifted by $\pi/2$ along ϕ -axis, one gets J_y^A curve. This is because, the system is symmetric under $\pi/2$ rotation in

absence of \vec{b} -field and \vec{b} -field alone dictates the direction and magnitude of the anomalous Josephson current since the phase bias is absent.

We next examine the behaviour of transverse critical Josephson currents with the Zeeman energy b in Fig. 5 for $\phi = \pi/4$, keeping other parameters unchanged. We can see from this figure that in the range $0 < b < 0.13t$, both J_y^{max} and J_y^{min} are of the same sign, which means the transverse Josephson current is unidirectional in this range. Such a behaviour changes as the system size is increased.

Summary and Conclusion .- A controlled SC phase difference can be experimentally applied in two-terminal Josephson junctions [28, 29]. With experimental advances in multi-terminal Josephson junctions [25, 30], the setup we propose should be within experimental reach.

To summarize, we have proposed a setup consisting of a SOC region connected to four SC terminals in a configuration that allows probing the planar Hall effect in Josephson currents by analyzing the response to a phase bias in the longitudinal direction. This setup enables simultaneous measurement of both longitudinal and transverse Josephson currents. We find that when the symmetry between k_x and $-k_x$ modes is broken, the system exhibits both the JDE and the AJE. Similarly, when the symmetry between k_y and $-k_y$ modes is broken, a finite transverse Josephson current emerges, with both AJE and JDE appearing in the transverse response. Notably, for certain parameter choices, the CPR exhibits unidirectional transport in the transverse direction, highlighting the potential for practical applications in superconducting devices.

Acknowledgements .- AS and BKS thank SERB Core Research grant (CRG/2022/004311) for financial support. AS thanks University of Hyderabad for funding through Institute of Eminence Professional Development Fund. BKS thanks the Ministry of Social Justice and Empowerment, Government of India, for a fellowship through NFOBC.

-
- [1] B. Josephson, Possible new effects in superconductive tunnelling, Phys. Lett. **1**, 251 (1962).
 - [2] A. Furusaki, Josephson current carried by andreev levels in superconducting quantum point contacts, Superlattices Microstruct. **25**, 809 (1999).
 - [3] F. Ando, Y. Miyasaka, T. Li, J. Ishizuka, T. Arakawa, Y. Shiota, T. Moriyama, and T. Ono, Observation of superconducting diode effect, Nature **584**, 373 (2020).
 - [4] C. Baumgartner, L. Fuchs, A. Costa, J. Picó-Cortés, S. Reinhardt, S. Gronin, G. C. Gardner, T. Lindemann, M. J. Manfra, P. E. Faria Junior, D. Kochan, J. Fabian, N. Paradiso, and C. Strunk, Effect of rashba and dreselhaus spin-orbit coupling on supercurrent rectification and magnetochiral anisotropy of ballistic Josephson junctions, J. Phys. : Condens. Matter **34**, 154005 (2022).
 - [5] B. Turini, S. Salimian, M. Carrega, A. Iorio, E. Strambini, F. Giazotto, V. Zannier, L. Sorba, and S. Heun, Josephson diode effect in high-mobility InSb nanoflags, Nano Lett. **22**, 8502 (2022).
 - [6] Y. Tanaka, B. Lu, and N. Nagaosa, Theory of giant diode effect in d -wave superconductor junctions on the surface of a topological insulator, Phys. Rev. B **106**, 214524 (2022).
 - [7] A. Soori, Nonequilibrium Josephson diode effect in periodically driven SNS junctions, Phys. Scr. **98**, 065917 (2023).
 - [8] A. Soori, Anomalous Josephson effect and rectification in junctions between Floquet topological superconductors, Physica E **146**, 115545 (2023).
 - [9] A. Costa, J. Fabian, and D. Kochan, Microscopic study

- of the Josephson supercurrent diode effect in Josephson junctions based on two-dimensional electron gas, *Phys. Rev. B* **108**, 054522 (2023).
- [10] B. Lu, S. Ikegaya, P. Buset, Y. Tanaka, and N. Nagaosa, Tunable Josephson diode effect on the surface of topological insulators, *Phys. Rev. Lett.* **131**, 096001 (2023).
- [11] D. Margineda, J. S. Claydon, F. Qejvanaj, and C. Checkley, Observation of anomalous Josephson effect in nonequilibrium Andreev interferometers, *Phys. Rev. B* **107**, L100502 (2023).
- [12] J. H. Correa and M. P. Nowak, Theory of universal diode effect in three-terminal Josephson junctions, *SciPost Phys.* **17**, 037 (2024).
- [13] S. Mondal, P.-H. Fu, and J. Cayao, Josephson diode effect with Andreev and Majorana bound states, [arXiv:2503.08318](https://arxiv.org/abs/2503.08318) (2025).
- [14] C. Goldberg and R. E. Davis, New galvanomagnetic effect, *Phys. Rev.* **94**, 1121 (1954).
- [15] H. X. Tang, R. K. Kawakami, D. D. Awschalom, and M. L. Roukes, Giant planar Hall effect in epitaxial (Ga,Mn)As devices, *Phys. Rev. Lett.* **90**, 107201 (2003).
- [16] A. Roy and P. S. A. Kumar, Giant planar Hall effect in pulsed laser deposited permalloy films, *J. Phys. D* **43**, 365001 (2010).
- [17] A. Annadi, Z. Huang, K. Gopinadhan, X. R. Wang, A. Srivastava, Z. Q. Liu, H. H. Ma, T. P. Sarkar, T. Venkatesan, and Ariando, Fourfold oscillation in anisotropic magnetoresistance and planar Hall effect at the LaAlO₃/SrTiO₃ heterointerfaces: Effect of carrier confinement and electric field on magnetic interactions, *Phys. Rev. B* **87**, 201102 (2013).
- [18] A. A. Taskin, H. F. Legg, F. Yang, S. Sasaki, Y. Kanai, K. Matsumoto, A. Rosch, and Y. Ando, Planar Hall effect from the surface of topological insulators, *Nat. Commun.* **8**, 1340 (2017).
- [19] D. Suri and A. Soori, Finite transverse conductance in topological insulators under an applied in-plane magnetic field, *J. Phys.: Condens. Matter* **33**, 335301 (2021).
- [20] A. Soori, Finite transverse conductance and anisotropic magnetoconductance under an applied in-plane magnetic field in two-dimensional electron gases with strong spin-orbit coupling, *J. Phys.: Condens. Matter* **33**, 335303 (2021).
- [21] E. V. Bezuglyi, A. S. Rozhavsky, I. D. Vagner, and P. Wyder, Combined effect of Zeeman splitting and spin-orbit interaction on the Josephson current in a superconductor–two-dimensional electron gas–superconductor structure, *Phys. Rev. B* **66**, 052508 (2002).
- [22] A. Rasmussen, J. Danon, H. Suominen, F. Nichele, M. Kjaergaard, and K. Flensberg, Effects of spin-orbit coupling and spatial symmetries on the Josephson current in SNS junctions, *Phys. Rev. B* **93**, 155406 (2016).
- [23] A. Costa and J. Fabian, Anomalous Josephson Hall effect charge and transverse spin currents in superconductor/ferromagnetic-insulator/superconductor junctions, *Phys. Rev. B* **101**, 104508 (2020).
- [24] O. Maistrenko, B. Scharf, D. Manske, and E. M. Hankiewicz, Planar Josephson Hall effect in topological Josephson junctions, *Phys. Rev. B* **103**, 054508 (2021).
- [25] N. Pankratova, H. Lee, R. Kuzmin, K. Wickramasinghe, W. Mayer, J. Yuan, M. G. Vavilov, J. Shabani, and V. E. Manucharyan, Multiterminal Josephson effect, *Phys. Rev. X* **10**, 031051 (2020).
- [26] A. Soori, Josephson diode effect in junctions of superconductors with band asymmetric metals, *J. Phys.: Condens. Matter* **36**, 335303 (2024).
- [27] A. Soori, Josephson diode effect in one-dimensional quantum wires connected to superconductors with mixed singlet-triplet pairing, *J. Phys.: Condens. Matter* **37**, 10LT02 (2025).
- [28] S. M. Frolov, D. J. Van Harlingen, V. A. Oboznov, V. V. Bolginov, and V. V. Ryazanov, Measurement of the current-phase relation of superconductor/ferromagnet/superconductor π Josephson junctions, *Phys. Rev. B* **70**, 144505 (2004).
- [29] J. A. Glick, V. Aguilar, A. B. Gougam, B. M. Niedzielski, E. C. Gingrich, R. Loloee, W. P. Pratt, and N. O. Birge, Phase control in a spin-triplet squid, *Sci. Adv.* **4**, eaat9457 (2018).
- [30] M. Gupta, G. V. Graziano, M. Pendharkar, J. T. Dong, C. P. Dempsey, C. Palmstrøm, and V. S. Pribiag, Gate-tunable superconducting diode effect in a three-terminal Josephson device, *Nat. Commun.* **14**, 3078 (2023).
- [31] A. Soori and M. Sivakumar, Nonadiabatic charge pumping across two superconductors connected through a normal metal region by periodically driven potentials, *J. Phys.: Condens. Matter* **32**, 365304 (2020).
-

Appendix A: Hamiltonian

Different terms that make up the Hamiltonian in eq. (1) are given below.

$$\begin{aligned}
H_L &= \sum_{n_x=1}^{L_s^x-1} \sum_{n_y=L_s^y+1}^{L_s^y} \left[-t(\Psi_{n_x+1,n_y}^\dagger \tau_z \Psi_{n_x,n_y} + h.c.) \right] + \sum_{n_x=1}^{L_s^x} \sum_{n_y=L_s^y+1}^{L_s^y-1} \left[-t(\Psi_{n_x,n_y+1}^\dagger \tau_z \Psi_{n_x,n_y} + h.c.) \right] \\
&\quad - \mu_s \sum_{n_x=1}^{L_s^x} \sum_{n_y=L_s^y+1}^{L_s^y} \Psi_{n_x,n_y}^\dagger \tau_z \Psi_{n_x,n_y} - \Delta \sum_{n_x=1}^{L_s^x} \sum_{n_y=L_s^y+1}^{L_s^y} \Psi_{n_x,n_y}^\dagger (\cos\phi_l \tau_y \sigma_y + \sin\phi_l \tau_x \sigma_y) \Psi_{n_x,n_y}, \\
H_{LS} &= -t_j \sum_{n_y=L_s^y+1}^{L_s^y} (\Psi_{L_s+1,n_y}^\dagger \tau_z \Psi_{L_s,n_y} + h.c.), \\
H_{SOC} &= \sum_{n_x=L_s^x+1}^{L_{sc}^x-1} \sum_{n_y=L_s^y+1}^{L_{sc}^y} \left[-t(\Psi_{n_x+1,n_y}^\dagger \tau_z \Psi_{n_x,n_y} + h.c.) \right] + \sum_{n_x=L_s^x+1}^{L_{sc}^x} \sum_{n_y=L_s^y+1}^{L_{sc}^y-1} \left[-t(\Psi_{n_x,n_y+1}^\dagger \tau_z \Psi_{n_x,n_y} + h.c.) \right] \\
&\quad - \mu_c \sum_{n_x=L_s^x+1}^{L_{sc}^x} \sum_{n_y=L_s^y+1}^{L_{sc}^y} \Psi_{n_x,n_y}^\dagger \tau_z \Psi_{n_x,n_y} + \frac{\alpha}{2} \sum_{n_x=L_s^x+1}^{L_{sc}^x} \sum_{n_y=L_s^y+1}^{L_{sc}^y-1} (i\Psi_{n_x,n_y+1}^\dagger \tau_0 \sigma_x \Psi_{n_x,n_y} + h.c.) \\
&\quad - \frac{\alpha}{2} \sum_{n_x=L_s^x+1}^{L_{sc}^x-1} \sum_{n_y=L_s^y+1}^{L_{sc}^y} (i\Psi_{n_x+1,n_y}^\dagger \tau_z \sigma_y \Psi_{n_x,n_y} + h.c.) + b \sum_{n_x=L_s^x+1}^{L_{sc}^x} \sum_{n_y=L_s^y+1}^{L_{sc}^y} \left[\Psi_{n_x,n_y}^\dagger (\cos\phi \tau_z \sigma_x + \sin\phi \tau_0 \sigma_y) \Psi_{n_x,n_y} \right], \\
H_{SR} &= -t_j \sum_{n_y=L_s^y+1}^{L_{sc}^y} (\Psi_{L_{sc}+1,n_y}^\dagger \tau_z \Psi_{L_{sc},n_y} + h.c.), \\
H_R &= \sum_{n_x=L_{sc}^x+1}^{L_{sc}^x-1} \sum_{n_y=L_s^y+1}^{L_{sc}^y} \left[-t(\Psi_{n_x+1,n_y}^\dagger \tau_z \Psi_{n_x,n_y} + h.c.) \right] + \sum_{n_x=L_{sc}^x+1}^{L_{sc}^x} \sum_{n_y=L_s^y+1}^{L_{sc}^y-1} \left[-t(\Psi_{n_x,n_y+1}^\dagger \tau_z \Psi_{n_x,n_y} + h.c.) \right] \\
&\quad - \mu_s \sum_{n_x=L_{sc}^x+1}^{L_{sc}^x} \sum_{n_y=L_s^y+1}^{L_{sc}^y} \Psi_{n_x,n_y}^\dagger \tau_z \Psi_{n_x,n_y} - \Delta \sum_{n_x=L_{sc}^x+1}^{L_{sc}^x} \sum_{n_y=L_s^y+1}^{L_{sc}^y} \Psi_{n_x,n_y}^\dagger (\cos\phi_r \tau_y \sigma_y + \sin\phi_r \tau_x \sigma_y) \Psi_{n_x,n_y}, \\
H_{BS} &= \sum_{n_x=L_s^x+1}^{L_{sc}^x} (\Psi_{n_x,L_s+1}^\dagger \tau_z \Psi_{n_x,L_s} + h.c.), \\
H_B &= \sum_{n_x=L_s^x+1}^{L_{sc}^x-1} \sum_{n_y=1}^{L_s^y} \left[-t(\Psi_{n_x+1,n_y}^\dagger \tau_z \Psi_{n_x,n_y} + h.c.) \right] + \sum_{n_x=L_s^x}^{L_{sc}^x} \sum_{n_y=1}^{L_s^y-1} \left[-t(\Psi_{n_x,n_y+1}^\dagger \tau_z \Psi_{n_x,n_y} + h.c.) \right] \\
&\quad - \mu_s \sum_{n_x=L_s^x+1}^{L_{sc}^x} \sum_{n_y=1}^{L_s^y} \Psi_{n_x,n_y}^\dagger \tau_z \Psi_{n_x,n_y} - \Delta \sum_{n_x=L_s^x+1}^{L_{sc}^x} \sum_{n_y=1}^{L_s^y} \Psi_{n_x,n_y}^\dagger \tau_y \sigma_y \Psi_{n_x,n_y}, \\
H_{ST} &= \sum_{n_x=L_s^x+1}^{L_{sc}^x} (\Psi_{n_x,L_{sc}+1}^\dagger \tau_z \Psi_{n_x,L_{sc}} + h.c.), \\
H_T &= \sum_{n_x=L_s^x+1}^{L_{sc}^x-1} \sum_{n_y=L_{sc}^y+1}^{L_{sc}^y} \left[-t(\Psi_{n_x+1,n_y}^\dagger \tau_z \Psi_{n_x,n_y} + h.c.) \right] + \sum_{n_x=L_s^x}^{L_{sc}^x} \sum_{n_y=L_{sc}^y+1}^{L_{sc}^y-1} \left[-t(\Psi_{n_x,n_y+1}^\dagger \tau_z \Psi_{n_x,n_y} + h.c.) \right] \\
&\quad - \mu_s \sum_{n_x=L_s^x+1}^{L_{sc}^x} \sum_{n_y=L_{sc}^y+1}^{L_{sc}^y} \Psi_{n_x,n_y}^\dagger \tau_z \Psi_{n_x,n_y} - \Delta \sum_{n_x=L_s^x+1}^{L_{sc}^x} \sum_{n_y=L_{sc}^y+1}^{L_{sc}^y} \Psi_{n_x,n_y}^\dagger \tau_y \sigma_y \Psi_{n_x,n_y},
\end{aligned} \tag{A1}$$

Here, $L_{sc}^d = L_s^d + L_c^d$ and $L_{scs}^d = 2L_s^d + L_c^d$, where $d = x, y$. The quantities L_s^d and L_c^d represent the number of sites

in the superconducting (SC) and spin-orbit-coupled (SOC) regions along direction d . The spinor Ψ_{n_x, n_y} is defined as

$$\Psi_{n_x, n_y} = \left[c_{n_x, n_y, \uparrow} \quad c_{n_x, n_y, \downarrow} \quad c_{n_x, n_y, \uparrow}^\dagger \quad c_{n_x, n_y, \downarrow}^\dagger \right]^T, \quad (\text{A2})$$

where $c_{n_x, n_y, \sigma}$ is the annihilation operator for an electron with spin σ at site (n_x, n_y) . The Pauli matrices $\tau_{x, y, z}$ and $\sigma_{x, y, z}$ act on the particle-hole and spin spaces, respectively. Other parameters include:

- t : hopping strength in the SC and SOC regions,
- t_j : hopping strength connecting the SC and SOC regions, chosen to be equal to t in our work,
- Δ : superconducting pairing strength,
- α : spin-orbit coupling strength,
- b : Zeeman energy,
- ϕ : angle between the Zeeman field and the x -axis,
- μ_s (μ_c): chemical potential in the SC (SOC) region.

Appendix B: Josephson currents

The Josephson current is given by the sum of currents carried by all occupied states [31]. Since charge is conserved in the SOC region, the charge current operators at four junctions between the SOC region and superconductors are:

$$\hat{J}_L = \frac{iet}{\hbar} \sum_{n_y=L_s^y+1}^{L_{sc}^y} (\Psi_{L_s+1, n_y}^\dagger \Psi_{L_s, n_y} - \text{h.c.}) \quad (\text{B1})$$

$$\hat{J}_R = \frac{iet}{\hbar} \sum_{n_y=L_s^y+1}^{L_{sc}^y} (\Psi_{L_{sc}+1, n_y}^\dagger \Psi_{L_{sc}, n_y} - \text{h.c.}) \quad (\text{B2})$$

$$\hat{J}_B = \frac{iet}{\hbar} \sum_{n_x=L_s^x+1}^{L_{sc}^x} (\Psi_{n_x, L_s+1}^\dagger \Psi_{n_x, L_s} - \text{h.c.}) \quad (\text{B3})$$

$$\hat{J}_T = \frac{iet}{\hbar} \sum_{n_x=L_s^x+1}^{L_{sc}^x} (\Psi_{n_x, L_{sc}+1}^\dagger \Psi_{n_x, L_{sc}} - \text{h.c.}) \quad (\text{B4})$$

For each ϕ_s , the eigenstates and eigenenergies ($|u_j\rangle, E_j$) of the Hamiltonian are obtained via numerical diagonalization. We assume that all negative energy states are occupied while positive energy states remain empty at $\phi_s \rightarrow 0^+$. At other values of ϕ_s , the occupied states are tracked by incrementally evolving them from the initially filled states.

The total Josephson current is given by

$$J_p = \sum_j \langle u_j | \hat{J}_p | u_j \rangle, \quad (\text{B5})$$

where $p = L, R, T, B$ and j is summed over occupied states.
